AIAA SciTech Forum
8–12 January 2018, Kissimmee, Florida
2018 AIAA Aerospace Sciences Meeting

10.2514/6.2018-0311

Optimal Tail Kinematics for Fish-Like Locomotion using the Unsteady Vortex Lattice Method

Ahmed A. Hussein* Saad Ragab † Haithem E. Taha‡ Muhammad R. Hajj†

The design of fish-like swimmers depends on understanding the interaction between the fluid motion and the body dynamics of the fish. Towards this objective, the optimal motion of the fish – tail is sought. As a simplified assumptions, the base body is assumed to be an elliptic shape while the tail is approximated as an Euler-Bernoulli beam. Three cases for the tail motion are considered in this paper. The first, second , and the third case are defined respectively as rigid beam, flexible beam in which the flexible motion is assumed to be a linear superposition of simple harmonic motions that have the shapes as the first and the second normal modes of the tail, and a flexible beam in which the flexible motion of the tail is determined by solving the fluid-structure coupled problem. In all three cases the input to the tail is pitching rotation at the root is to be determined by minimizing the hydrodynamic power subjected to zero net thrust on the fish body. The unsteady hydrodynamic loads are calculated using the two-dimensional unsteady vortex lattice method. The aim of the study is to investigate the effect of the tail active and passive flexibility on the propulsive efficiency versus the rigid tail.

Nomenclature

a	Semi-chord length
E	Modulus of elasticity of the tail
r_k	Position of the vortex shed from the tail trailing edge
θ_{max}	Maximum pitching angle of the tail
ρ_m	Density of tail
Φ	Phase shift between the first two mode shapes of Euler-Bernoulli beam
Γ_{b_i}	Strength of the ith bound vortex
Γ_{w_k}	Strength of the kth wake vortex
Ψ_i	The ith mode shape of Euler-Bernoulli beam
ν	Poisson ratio of the tail
$\lvert\Psi_i\rvert$	magnitude of ith mode shape

*PhD student,Department of Biomedical and Engineering Mechanics, Virginia Tech., Blacksburg
†Professor, Department of Biomedical and Engineering Mechanics, Virginia Tech., Blacksburg
‡Assistant Professor, Department of Mechanical and Aerospace Development, University of California, Irvine

I. Introduction

Motivated by the desire to understand and characterize fish, engineers have long considered modes of such motions to inspire the design and improvement technologies for human need. Earlier considerations of the nature of fish propulsion have been brought into attention by Lindsey [1], that was followed by more detailed work by Borelli [2]. The interest in understanding the generation of propulsive forces was mainly inspired by impressive structural and kinematic capabilities. Further detailed work since Borelli has been diversified, with descriptions shared by Sir James Gray (1933a–c), Lighthill [3], Webb Blake [4], Maddock et al. [5], and Triantafyllou et al. [6] among others. Published literature included experimentally and analytically detailed analyses of patterns of body, morphological adaptations and their effects on flow patterns that have helped scientists understand how propulsion is produced.

In swimming, fish vary their shape to generate fluid dynamic forces needed for propulsion and control. The oscillating tails and fins are able to generate additional thrust, and may also be used to balance roll and yaw moments generated during locomotion. Our ultimate goal is to develop an understating of the underlying physics of fish locomotion based on a three-dimensional potential flow model that can be used to support a geometrically controlled framework for the design and control of pisciform swimmers. This would be achieved using periodically forced mechanical systems, and compromised of a series of rigid airfoil and flaps. The ultimate question to be answered is: For what parameter values (Reynolds number, frequency of oscillation, number of links, and model parameters) will the proposed unsteady flow model capture forces and moments with sufficient accuracy to support geometric control design and analysis?

Towards that objective, we investigate the optimal kinematics of fish-tail motion. As a first step, we consider the oscillatory type of fish in two dimensions. In this case, the base body is considered as a rigid part and the tail is allowed to flap either flexibly or rigidly. The flexible motion of the tail is modeled in a two different ways. The first one the flexible motion of the tail assumed to be a combination of a simple harmonic motions in time using the first two mode shapes of Euler-Bernoulli beam. The second on the flexible motion of the tail is determined by solving the fluid-structure coupled problem defined in Equations 1 and 2. The hydrodynamic loads is calculated using the two-dimensional unsteady vortex lattice model (UVLM). The propulsive efficiency versus the Strouhal Number is depicted for the three cases.

II. Geometrical Model of the Tail

The two-dimensional fish is modeled as a two bodies connected at one point as shown in Figure [1]. The base body and tail are modeled as a rigid ellipse and a flexible beam respectively. The body and the tail are moving with the same uniform velocity U_∞. The input to the tail is angular displacement $\theta(t)$, and is to be determined by minimizing the hydrodynamic power subjected to zero net thrust on the fish body. For the rigid beam case the deflection w is neglected, i.e. $w = 0$, while for the first flexible case, active flexibility, it is taken to be a simple harmonic combination of the first and second modes of the beam [7] as

$$w(x,t) = A_1 sin(\omega t)\Psi_1(x) + A_2 sin(\omega t + \Phi)\Psi_2(x) \tag{1}$$

where A_1 and A_2 are the amplitude of the first and second mode respectively, and ω is the frequency of oscillation, i.e. $\omega = 2\pi f$. For the case of passive flexible beam, the tail deflection is determined as follows. The position of a general point $\boldsymbol{P}$ on the tail and the angular velocity of the tail can be defined as

$$\vec{r_p} = x\hat{\boldsymbol{i}} + w\hat{\boldsymbol{k}} \tag{2}$$

$$\vec{\omega} = \dot{\theta}\hat{\mathbf{j}} \tag{3}$$

The inertial velocity and accelration can be computed as follows :

$$\begin{aligned} \vec{\mathbf{V}} = \frac{d\vec{\mathbf{r}_p}}{dt} &= \frac{\partial \vec{\mathbf{r}_p}}{\partial t} + \vec{\omega} \times \vec{\mathbf{r}_p} \\ &= \dot{\theta} w \hat{\boldsymbol{i}} + \left(\dot{w} - \dot{\theta} x\right)\hat{\boldsymbol{k}} \end{aligned} \tag{4}$$

$$\begin{aligned} \vec{\mathbf{a}} = \frac{d\vec{\mathbf{V}}}{dt} &= \frac{\partial \vec{\mathbf{V}}}{\partial t} + \vec{\omega} \times \vec{\mathbf{V}} \\ &= \left(\ddot{\theta} w + 2\dot{\theta}\dot{w} - \dot{\theta}^2 x\right)\hat{\boldsymbol{i}} + \left(\ddot{w} - \ddot{\theta} x - \dot{\theta}^2 w\right)\hat{\boldsymbol{k}} \end{aligned} \tag{5}$$

Applying the equilibrium conditions on a general element centered at the point $\boldsymbol{P}$ in x and z directions, we get

$$T(x) = \frac{m\dot{\theta}^2}{2}(R^2 - x^2) + m\int_x^R \left(\ddot{\theta}w + 2\dot{\theta}\dot{w}\right) dx \tag{6}$$

$$\frac{\partial^2}{\partial x^2}\left(EI\frac{\partial^2 w}{\partial x^2}\right) - \frac{\partial}{\partial x}\left(T(x)\frac{\partial w}{\partial x}\right) + m\left(\ddot{w} - \ddot{\theta}x - \dot{\theta}^2 w\right) = F_H(w) \tag{7}$$

The instantaneous tail dispacement $w(x,t)$ is determined by the solving the fluid-structured equations of motion defined in Eq.(6) and Eq.(7) according to the flowchart shown in Figure 3. $T(x)$ is the tension in the tail due to the angular rotation $\theta(t)$. E and I are the modulus of elasticity and moment of inertia of the tail respectively. $F_H(w)$ is the external hydrodynamic loads generated on the tail by the motion θ. The structural and hydrodynamic loads are coupled through the presence of the variable $w(x,t)$ in both sides. The calculation of the hydrodynamic loads is defined in the next section.

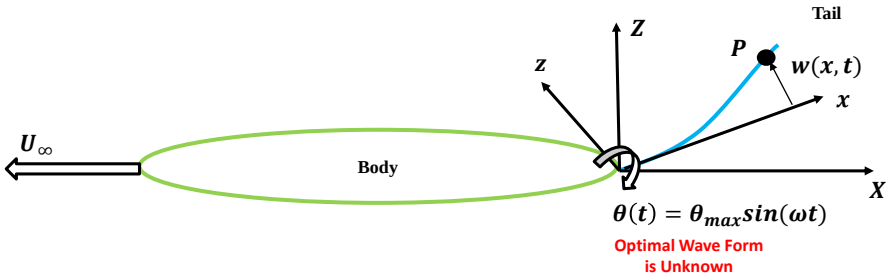

Figure 1: Simple model of the fish-tail of oscillatory type.

III. Hydrodynamic Model

The hydrodynamic forces and moments generated by the tail motion are calculated using the unsteady vortex lattice method (UVLM) [8, 9, 10, 11, 12, 13, 14]. The tail section can move and rotate with a velocity $\boldsymbol{V}$ and angular velocity $\dot{\theta}$ respectively. As shown if Figure [2a], the tail is replaced by a vortex sheet of N bound vortices Γ_{b_i}. At each time step, a vortex is released from the trailing edge Γ_{w_i}. The Kutta condition is satisfied by placing the vortex at the quarter chord of each panel and applying the no-penetration boundary condition at the three quarter point of each panel [10, 14]. the strength of the shed vortex is determined by applying Kelvin circulation theorem at each time step, i.e. $d(\sum_{i=1}^{N}\Gamma_{b_i} + \sum_{i=1}^{N_w}\Gamma_{w_i})/dt = 0$. The drag force acting on the base body is assumed to be constant based on a drag coefficient of $C_D = 0.0018$.

IV. Finite Element Model of the Coupled Problem

The finite element approach was applied to Eq.(7). The nonlinear term in the tension $T(x)$ is neglected [15], i.e. $T(x) \approx m\dot{\theta}^2(R^2 - x^2)/2$. The resulting equations are nonlinear time-varying of the form:

$$[\mathbf{M}]\{\ddot{\mathbf{q}}\} + [\mathbf{K}]\{\mathbf{q}\} = \{\mathbf{F(q)}\} \tag{8}$$

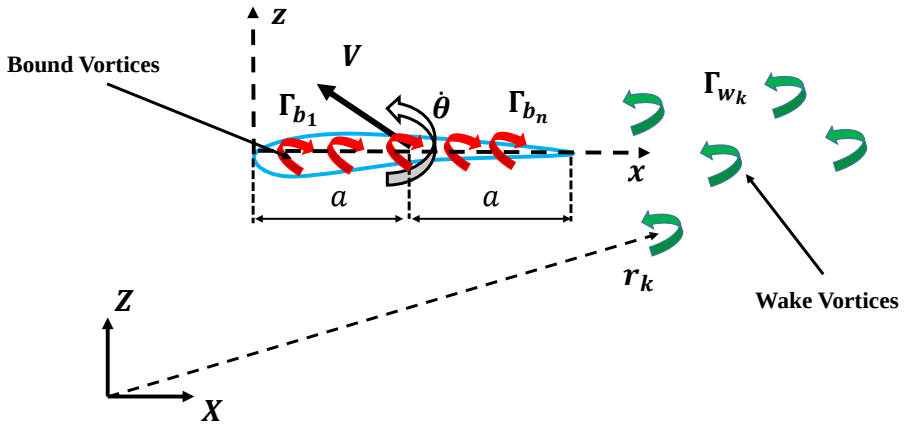

a) Two dimesnional UVLM

Figure 2: Discrete vortex model of fish the tail.

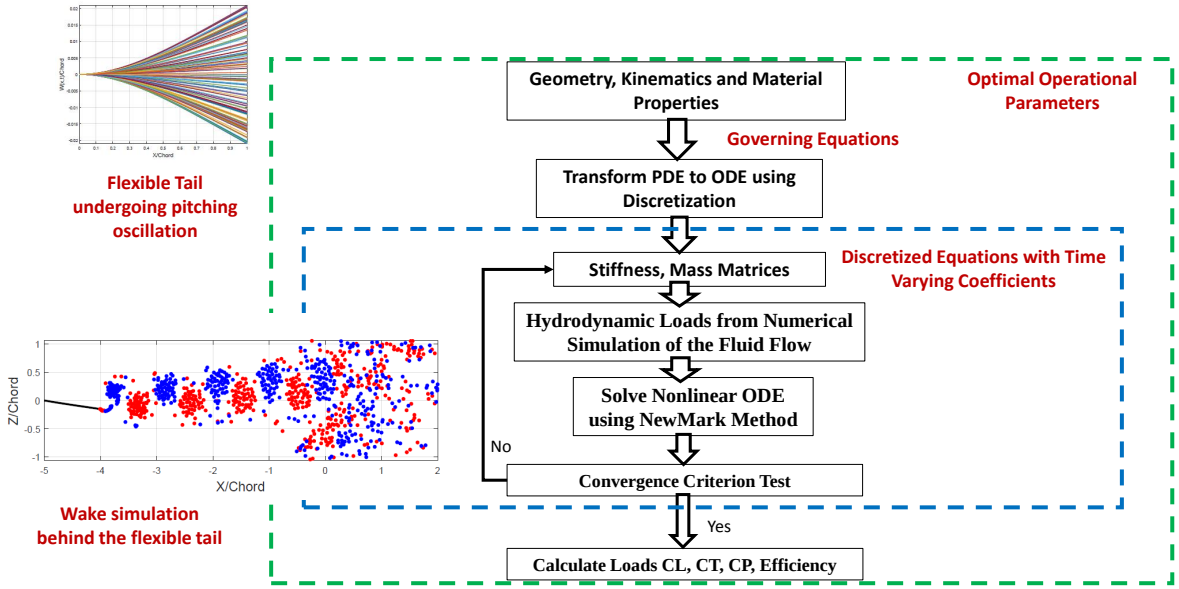

Figure 3: Flowchart for the solution of UVLM

where $[\mathbf{M}]$ is the mass matrix $[\mathbf{K}]$ is the stiffness matrix, and $\{\mathbf{F}(\mathbf{q})\}$ is the time-dependent forcing vector containing terms that are dependent of the nodal degrees of freedom $\mathbf{q}$ resulting from the UVLM and the inertia loads. Hermite polynomials are used to represent the distribution of $\mathbf{q}$ over one element [16] with two degrees of freedom at each

node, i.e. $\mathbf{q} = \{w \quad \partial w/\partial x\}^T$. The coupling between the structure and the hydrodynamic loads appears in $\boldsymbol{F}_H(\boldsymbol{q})$ determined using the UVLM. At each time step, an initial position of the tail motion $\boldsymbol{q}(t_0^k)$ is assumed. Then the hydrodynamic loads are calculated based on this configuration. A local iteration is performed until the difference between two successive tail configurations are within the defined convergence criteria, i.e. $|\boldsymbol{q}(t_{m+1}^k) - \boldsymbol{q}(t_m^k)| < \epsilon$. Then the tail configuration at the next time step is set to be the one form the last local iteration, i.e. $\boldsymbol{q}(t_0^{k+1}) = \boldsymbol{q}(t_{m+1}^k)$. The procedure used for the local iteration and solving for the instantaneous tail position w is shown in Figure 3. Newmark method [17] is used to integrate the equations of motion (8) in time with integration parameter $\alpha = 0.6$. the effect of varying this parameter will be addressed in future work.

V. Numerical Data and Assumptions

In this study, we made some assumptions to simplify the problem. For the case of the active flexible beam, the input $\theta(t)$ and the harmonic term in the deflection $w(x,t)$ have the same frequency ω. This is not the situation in a general case. In future work, an independent function of time will be assigned to each motion. The values of the tail geometry and material properties, aluminum, used in this study are defined in Table 1. A convergence curve for the 2D-UVLM is shown in Figure 4. Based on this results, we choose the panel size to be $dx = Chord/50$ and time step to be $dt = 2\pi/(\omega 100)$.

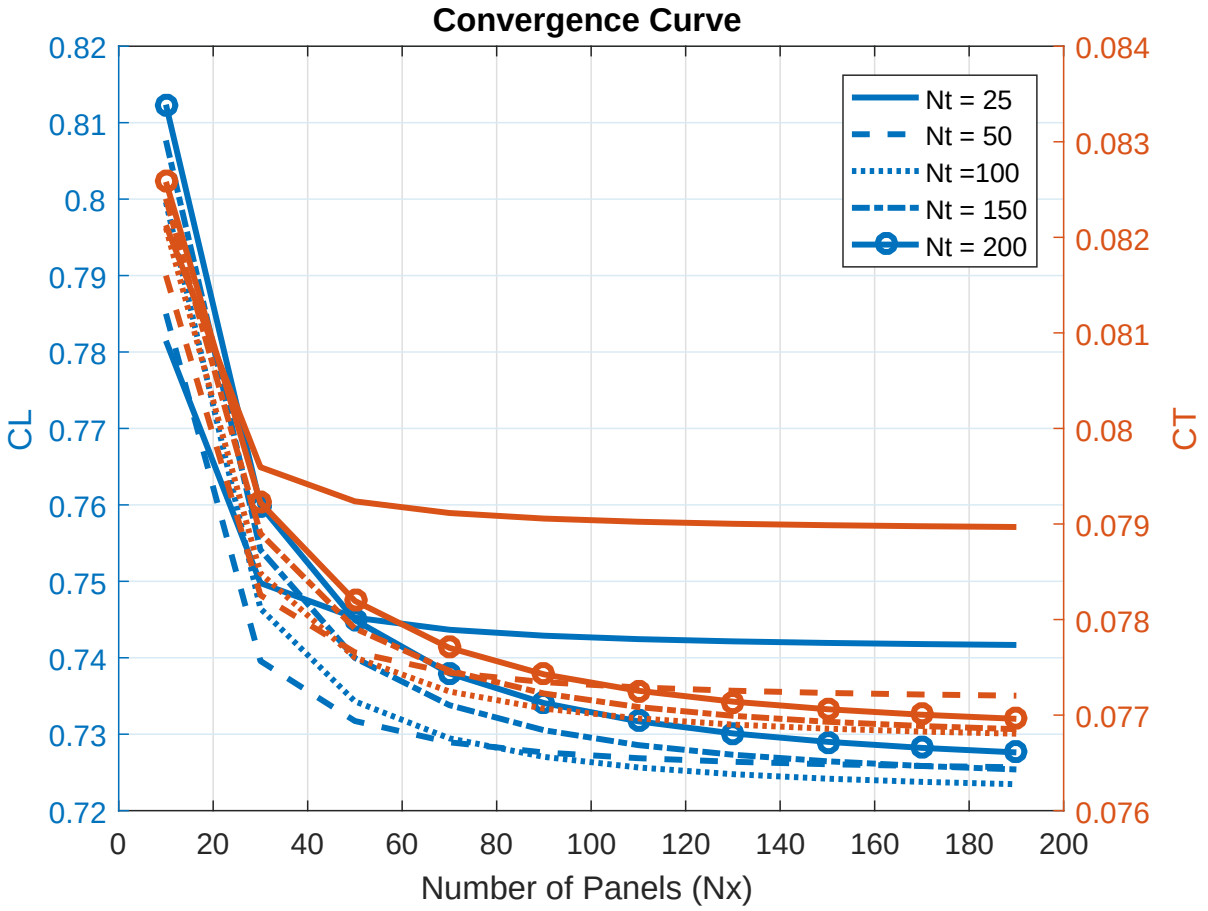

a) Lift and thrust coefficeients versus number of panels for different time steps.

Figure 4: Convergence curves for the two-dimensional UVLM

Table 1: Parameters Value

$Chord$	$150\ mm$	Span	$50\ mm$
t	$2.7\ mm$	E	$69\ GPa$
ρ_m	$2750\ kg/m^3$	ν	0.3
θ_{max}	7.2^o		

VI. Results

Figure [5] shows the thrust efficiency defined as a percentage of the input power for different cases of rigid and active and passive flexible tails. The results show that mode 2 forcing yield the highest efficiency near Strouhal number of $St = 0.15$. In comparison mode 1 yields the lowest efficiency. The passive flexible tail yields an efficiency more than rigid case. Also the case of adding the two modes does not improve the efficiency. In future work, a range of flexible tails will be considered to investigate the effect of flexibility on the efficiency and if a certain mode can be excited to achieve more thrust efficiency.

The time histories of the lift, thrust, and power coefficients at the optimal efficiency for the three cases are depicted in Figure [6] over five flapping cycles. Achieving steady-state solution is noted, which implies that the solution can be used for comparing its performance with other configurations. In Figure [7], the wake generated by the fish tail is shown for the three cases. The red and blue indicates clockwise and anti-clockwise vortices respectively. This behviour has shown by Willis [18] to be the the same pattern of von Kármán street but of opposite signs of the wake vortices. The von Kármán street pattern of the wake vortices indicates that the net horizontal force is drag. In contrast, when the signs of the wake vortices switched as in the present case in Figure [7], the net horizontal force is thrust. The difference between the wake structure between the different cases is hard to distinguish which is expected because the amplitude of the oscillations is maintained constant for all cases. In future, we will examine the level of vorticity generated by the different configurations.

Conclusion

In this paper, the propulsive efficiency is compared for three cases of the fish-tail. The cases are rigid, active flexible, and passive flexible beam respectively. The results showed that optimal efficiency is achieved for the case of the active flexible beam with the second mode. On the other hand, the passive flexible beam have more optimal efficiency than the rigid one but less than that of the tail excited with the second mode. The future plan is to assign an independent function for the rigid body rotation, and the first and second mode through an optimization frame work to determine the optimum parameters. Based on these optimization results, we will design the tail flexibility such that the mode that gives high efficiency is excited.

References

[1] CC Lindsey. 1 form, function, and locomotory habits in fish. *Fish physiology*, 7:1–100, 1979.

[2] M Bozkurttas, R Mittal, H Dong, GV Lauder, and P Madden. Low-dimensional models and performance scaling of a highly deformable fish pectoral fin. *Journal of Fluid Mechanics*, 631:311–342, 2009.

[3] Sir James Lighthill. *Mathematical biofluiddynamics*. SIAM, 1975.

[4] PW Webb and RW Blake. Swimming. in functional vertebrate morphology, 1983.

[5] Linda Maddock, Quentin Bone, and Jeremy MV Rayner. *The Mechanics and Physiology of Animal Swimming*. Cambridge University Press, 1994.

[6] George S Triantafyllou, MS Triantafyllou, and MA Grosenbaugh. Optimal thrust development in oscillating foils with application to fish propulsion. *Journal of Fluids and Structures*, 7(2):205–224, 1993.

[7] Junuthula Narasimha Reddy. *An introduction to the finite element method*, volume 2. McGraw-Hill New York, 1993.

[8] SM Belotserkovskii. Study of the unsteady aerodynamics of lifting surfaces using the computer. *Annual Review of Fluid Mechanics*, 9(1):469–494, 1977.

[9] C Rehbach. Numerical calculation of three-dimensional unsteady flows with vortex sheets. In *16th Aerospace Sciences Meeting*, page 111, 1978.

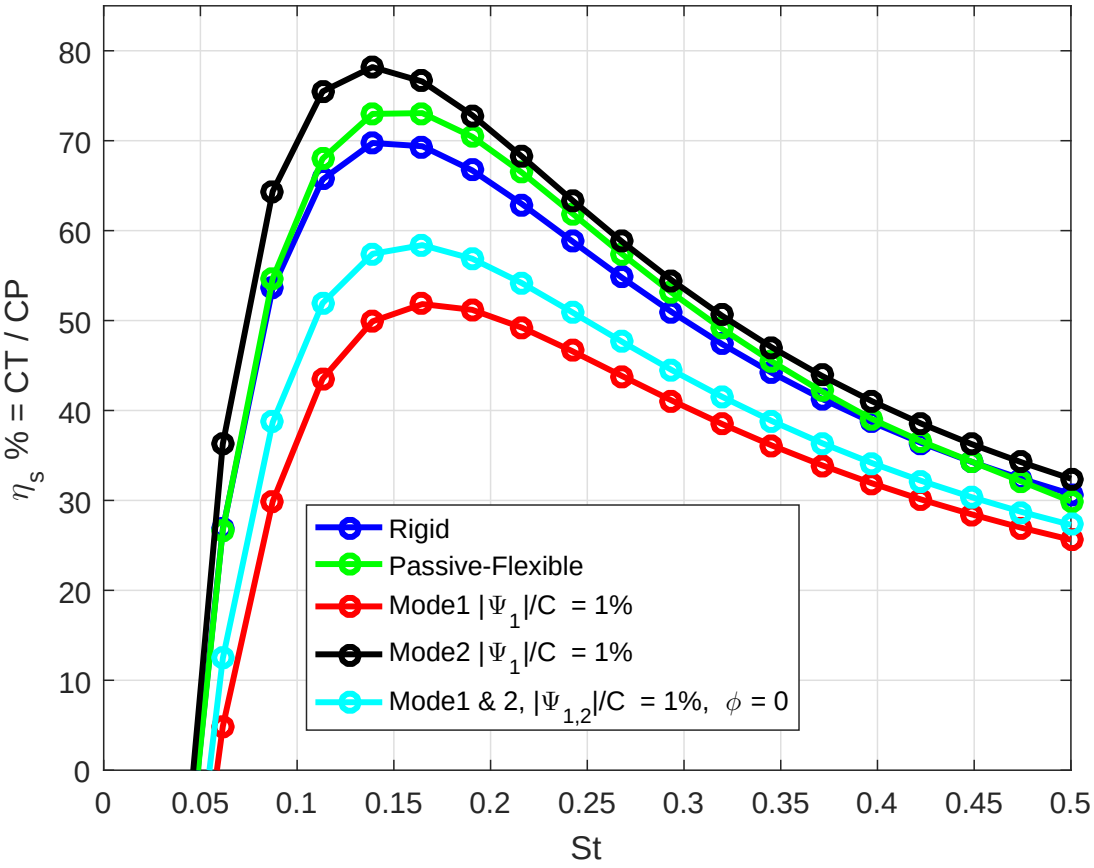

a) Propulsive Efficiency η_s for different tail cases.

Figure 5: Propulsive Efficiency versus Strouhal number.

[10] EH Atta, OA Kandil, DT Mook, and AH Nayfeh. Unsteady aerodynamic loads on arbitrary wings including wing-tip and leading-edge separation. *AIAA*, 156:1977, 1977.

[11] P Konstadinopoulos, DF Thrasher, DT Mook, AH Nayfeh, and L Watson. A vortex-lattice method for general, unsteady aerodynamics. *Journal of aircraft*, 22(1):43–49, 1985.

[12] Daniel Levin and Joseph Katz. Vortex-lattice method for the calculation of the nonsteady separated flow over delta wings. *Journal of Aircraft*, 18(12):1032–1037, 1981.

[13] Joseph Katz. Lateral aerodynamics of delta wings with leading-edge separation. *AIAA journal*, 22(3):323–328, 1984.

[14] Joseph Katz and Allen Plotkin. *Low-speed aerodynamics*, volume 13. Cambridge University Press, 2001.

[15] D H Hodges and E H Dowell. Nonlinear equations of motion for elastic bending and torsion of twisted non-uniform rotor blades. Technical report, Dec.1974.

[16] Maeng Hyo Cho and In Lee. Aeroelastic stability of hingeless rotor blade in hover using large deflection theory. *AIAA Journal*, 32(7):1472–1477, 1994.

[17] Nathan M Newmark. A method of computation for structural dynamics. *Journal of the engineering mechanics division*, 85(3):67–94, 1959.

[18] Jay Willis. Wake sorting, selective predation and biogenic mixing: potential reasons for high turbulence in fish schools. *PeerJ*, 1:e96, 2013.

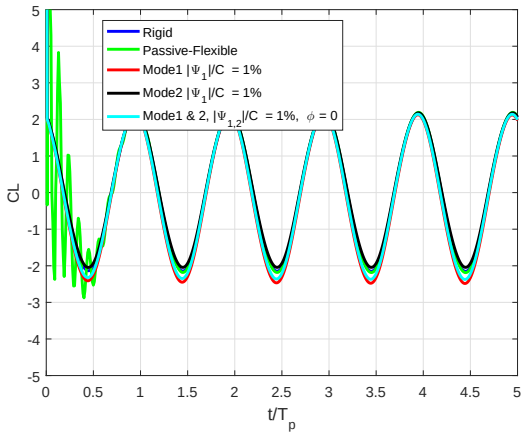

a) Lift coefficeint versus time.

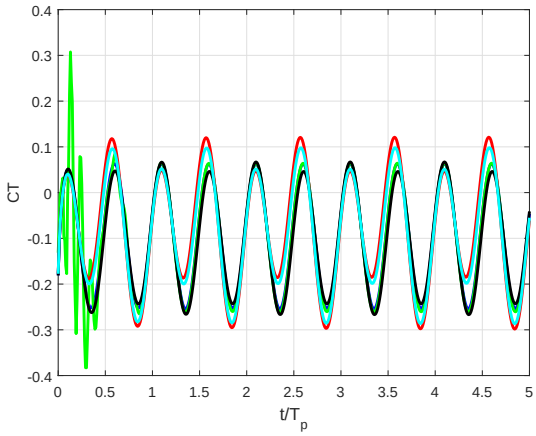

b) Thrust coefficeint versus time.

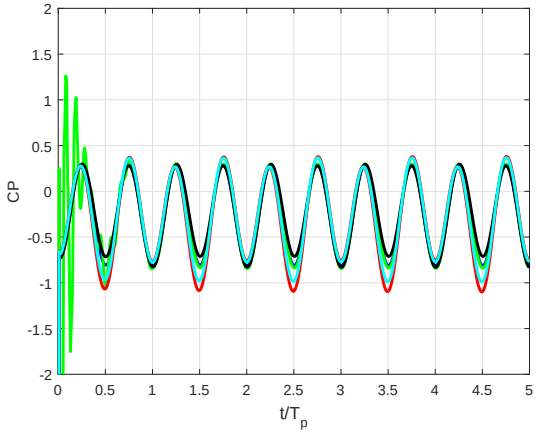

c) Power coefficeint versus time.

Figure 6: Time history of lift, thrust and power coefficients at optimal Strouhal number for the last two pitching cycles.

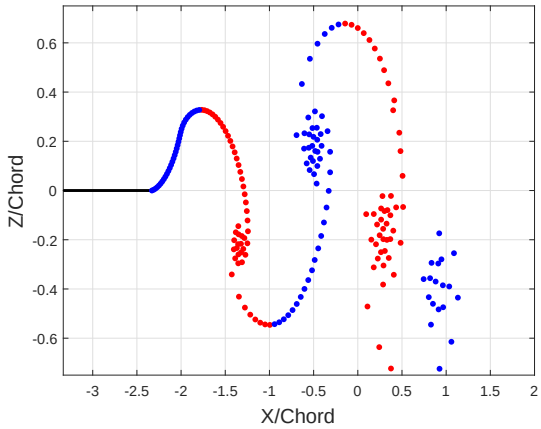

a) Wake pattern behind the fish-tail for the rigid beam.

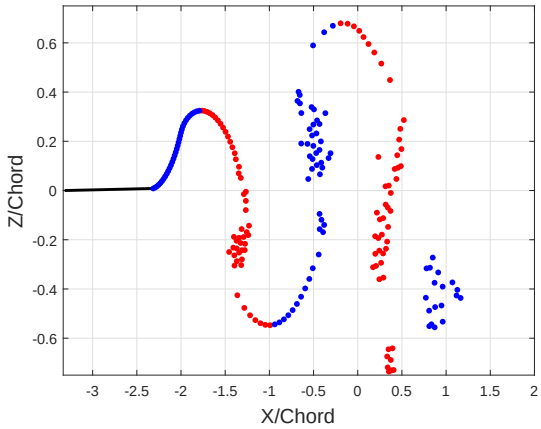

b) Wake pattern behind the fish-tail for the passive flexible beam.

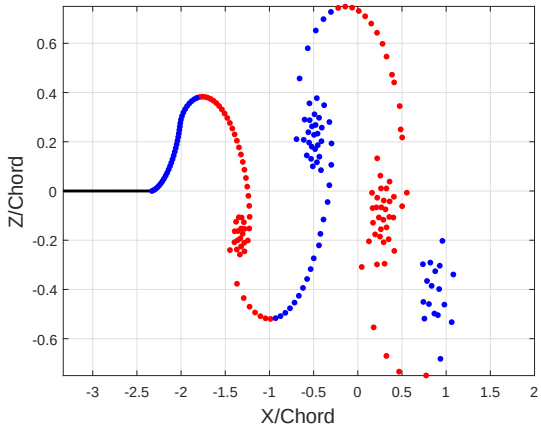

c) Wake pattern behind the fish-tail for the active beam with the first mode.

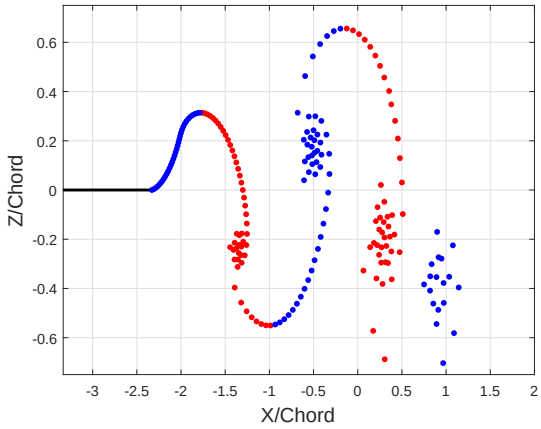

d) Wake pattern behind the fish-tail for the active beam with the second mode.

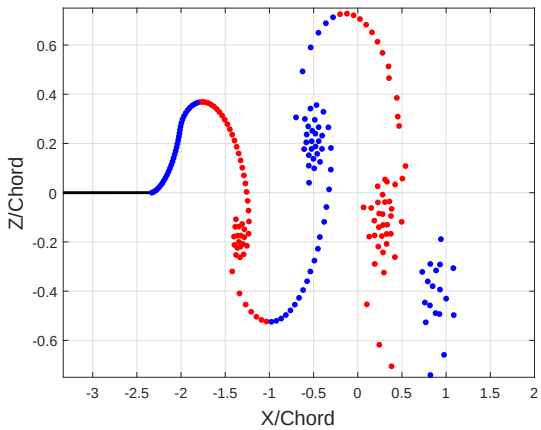

e) Wake pattern behind the fish-tail for the active beam with the second mode.

Figure 7: Wake pattern behind the fish-tail for the rigids, passive, and active flexible beam